2018 26th Mediterranean Conference on Control and Automation (MED)
Zadar, Croatia, June 19-22, 2018

Position Tracking and Control of Lightweight Flexible Joint Manipulator Robolink® using Kinect Sensor

Ioannis Stathopoulos, Foivos Papandreou and Stamatios Manesis, Member, IEEE

Abstract — **In this article, a method of feedback data acquisition and target recognition using Kinect sensor is proposed, in order to perform position tracking and control of Robolink® articulated arm. Robolink is a lightweight flexible joint robotic manipulator, the rotational joints of which are driven by step motors through Dyneema wires. The goal of the presented experimental work was to investigate the possibility to use Robolink in fruit picking systems and other similar works. At an early stage, Lidar sensors were also used for Robolink indoor behavior experimentation. Feedback data management and control law, based on the kinematics of this lightweight flexible robotic arm are also analyzed and presented from the efficiency point of view.**

I. Introduction

Lightweight robotic manipulators are extensively imported in automation field. The high load to arm weight ratio and the ability to perform high-speed tasks are mainly the reasons that lightweight robots form an integral part of wide application areas and science researches. Joint elasticity is an inherent characteristic of them, that directly effects on robot kinodynamic performance by including parameters of uncertainty as has been proposed by [1].

Researches in flexible robots have been conducted to implement control theory and design with the aim of approaching each desired operation. Significant researches based on adaptive control techniques [2-4] have been developed in accordance with parametrical elasticity, which is a feature that makes the model more complex. In the same direction of assessing the flexibility phenomenon, neural networks strategies [5-8] have been proposed to control flexible-joint robots. Both aforementioned approaches are confronted with the lack of certainty in measuring joint flexibility. To overcome this issue, parameters identification and calibration have been an objective of specific research in [9]. In contrast, prescribed performance control for flexible joint robots is a method that fulfills the desired standards without any knowledge on robot dynamics and elasticity parameters [10].

Feedback data are essentials when closed loop control systems are implemented. Some researches, in order to minimize experimental measurements, have been concentrated on reducing the number of feedback quantities. Some models propose the estimation of link-motor position and velocity [11-13] while others are focused on position and torque feedback [14-16]. In some cases based on state observers, measuring only the position has proven to be adequate [17-19].

The principles of fruit picking robots, as shown in Fig. 1, have been developed since the early 1980's and primary research was carried out to determine system capabilities required to harvest fruit more efficiently than an experienced human picker. Significant work has since been done both in the construction of complex robotic mechanisms for fruit picking [20-24], and in the development of vision based techniques for fruit recognition and manipulator control [25-27]. An original choice of authors was to use a commercial single-set vision-based measurement system as low cost as possible, such as the Kinect sensor.

To develop the closed-loop control laws, sensor systems are being constantly upgraded with the view of measuring in a more accurate manner. Science community often attempts to modify technologies that are primarily constructed for different usage. After having recognized the significance of position tracking, two different stages of project's task approaching for joint's kinetic parameters and target recognition were followed. Both are described in this paper and being used to provide the feedback data needed for control system. Based on desired and real joint signals, position control is being performed. More advanced types of control, such as velocity or torque control, are beyond the scope of this paper. Experimental validation was realized under the lightweight flexible joint Robolink® articulated arm by igus® GmbH, during the first stage through Lidar-Programmable Logic Controller (PLC) and during the second stage Kinect-LabVIEW setups.

Figure 1. Flexible robots can be used as fruit pickers.

In section II, the kinematic model of Robolink is analyzed. The problem of both forward and inverse kinematics are defined and solved. Section III presents both Lidar-based and Kinect-based approaches of feedback data acquisition and manipulation. Control schemes and experimental cases are described in section IV. The contribution of this work is summarized in section V.

II. Kinematic Analysis

A. Forward Kinematics

Initially, the forward kinematics analysis of the articulated arm, on which the experimental procedure is

The authors are with the Electrical and Computer Engineering Department, University of Patras, GR-26500 Rio, Achaia, Greece, (e-mail: ioannis.stath@gmail.com, foivos.papandreou@outlook.com.gr, stam.manesis@ece.upatras.gr)

based, is presented.

Main structural parts of the Robolink robotic manipulator are its joints (Fig. 2a). Each joint is placed at the edge of an aluminum link and it is followed by another one of the same material. The total arrangement is consisted of two joints and three links (Fig. 2b). The first link is fixed and its lower point is considered as the 3D space origin. The end of the last link is considered as the end effector.

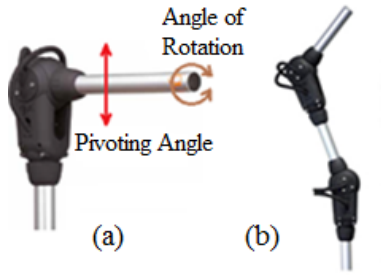

Figure 2. The 2-DoF joint and each angle of movement are depicted in (a), and a 2-joint system arrangement is shown in (b).

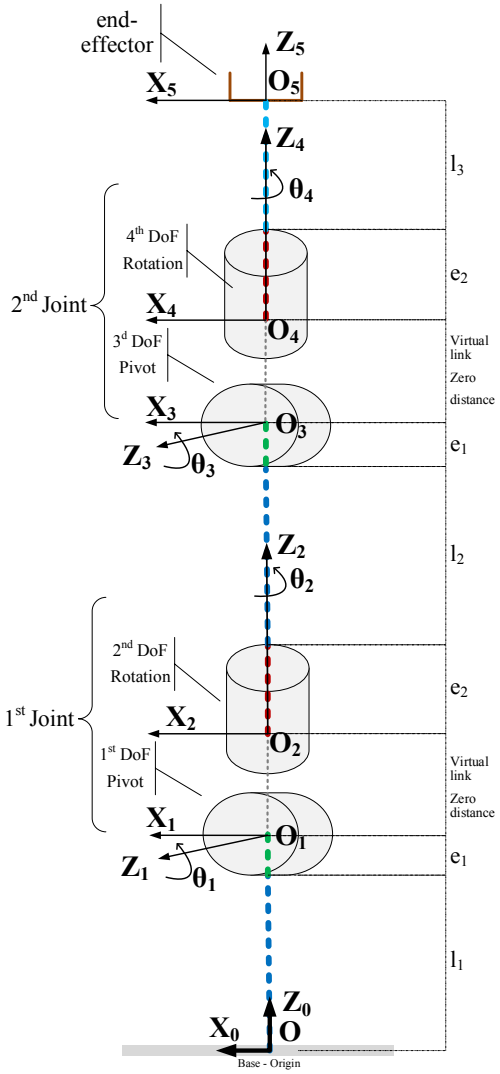

Figure 3. Definition of each Coordinate System.

TABLE I. DENAVIT HARTENBERG PARAMETERS

Link i	α_i	d_i	a_i	θ_i
1	0	l_1+e_1	-90°	0
2	0	0	90 °	θ_1
3	0	$e_2+l_2+e_1$	-90 °	θ_2
4	0	0	90 °	θ_3
5	0	e_2+l_3	0	θ_4

The joint is made of specific plastic material and each axial movement is driven by Dyneema wires attached to a step motor. Consequently, stiffness of the joint is reduced contrary to its flexibility. This 2 Degrees of Freedom (DoF) revolute joint is able to perform movement over a pivoting angle and an angle of rotation. To analyze the kinematic performance of the joint, a virtual link of zero length is hypothetically inserted to its main body so as to be described as a couple of 1-DoF joint.

Denavit–Hartenberg (DH) convention expresses the mathematical relation between the coordinated frames [28], which are defined with respect to each axis of movement as shown in Fig. 3. Hence, end effector's position and orientation are represented with reference to the origin coordinate system. It should be denoted that the first link does not introduces additional degrees of freedom into the model. However, DH representation simplifies the expressions in a more parametrical manner (Table I), where l_i is the length of each link respectively, e_1 is the distance between the end of the previous link and the center of rotation and e_2 is the distance from the center of rotation of the joint to the beginning of the next link. θ_i is the angle of each DoF, for $i \in \{1,3\}$ $\theta_i \in [-90°, 90°]$ and for $i \in \{2,4\}$ $\theta_i \in [-170°,170°]$.

The universal transformation is described by the 4x4 matrix $T=\begin{bmatrix} R & w \\ 0 & 1 \end{bmatrix}$ where R is the 3x3 sub-matrix of orientation and $w=[x \quad y \quad z]^T$ is the vector of the end effector position,

$$w=\begin{bmatrix} C_1\sin\theta_1+C_2(\sin\theta_1\cos\theta_3+\cos\theta_1\cos\theta_2\sin\theta_3) \\ C_2\sin\theta_2\sin\theta_3 \\ C_1\cos\theta_1+C_2(\cos\theta_1\cos\theta_3-\sin\theta_1\cos\theta_2\sin\theta_3)+C_3 \end{bmatrix} \quad (1)$$

where each constant variable is defined as follows $C_1=e_1+e_2+l_2$, $C_2=e_2+l_3$ and $C_3=e_1+l_1$.

As it is obtained from (1), the end effector position is not related with the rotation angle of the last joint. Given the values for each length l_i: $l_1=l_2=0.64$m, $l_3=0.54$m and each distance e_i: $e_1=0.135$m, $e_2=0.065$m, the workspace of the manipulator can be easily calculated. In general, since the length of each link can be selected by the user, the Robolink's workspace could be dimensionally adopted to the specific type of tree, the fruits of which are expected to be picked.

B. Inverse Kinematics

In this section, the problem of inverse kinematics is solved given only the position $[x\ y\ z]^T$ of the end effector of Robolink. According to the forward kinematics $\theta_3=\varphi_1(x,y,z)$ can be obtained from (2),

$$\theta_3 = \pm \arccos \frac{x^2+y^2+(z-C_3)^2-C_1^2-C_2^2}{2C_1C_2} \quad (2)$$

Following, $\theta_2=\varphi_2(\theta_3,x,y,z)$ is calculated from (3) based on the y-coordinate of position vector (1),

$$\theta_2 = \pm \arcsin \frac{y}{C_2 \sin\theta_3} \quad (3)$$

Consequently, four sets of solutions are obtained for each combination of (θ_2, θ_3). As far as $\theta_1=\varphi_3(\theta_2,\theta_3,x,y,z)$ is concerned, it is uniquely defined as follows. As stated in (1) for z-coordinate,

$$z=C_1\cos\theta_1+C_2\cos\theta_1\cos\theta_3-C_2\sin\theta_1\cos\theta_2\sin\theta_3+C_3$$

$$\cos\theta_1=\frac{z-C_3}{C_1+C_2\cos\theta_3}+\frac{C_2\cos\theta_2\sin\theta_3}{C_1+C_2\cos\theta_3}\sin\theta_1 \quad (4)$$

Substitution of (4) to x-coordinate of (1) derives,

$$\sin\theta_1=\frac{x(C_1+C_2\cos\theta_3)+(C_3-z)C_2\cos\theta_2\sin\theta_3}{(C_1+C_2\cos\theta_3)^2+(C_2\cos\theta_2\sin\theta_3)^2} \quad (5)$$

and thus,

$$\theta_1=\text{atan2}(\sin\theta_1,\cos\theta_1) \quad (6)$$

It should be noticed that when θ_3 is equal to zero, θ_2 cannot be singularly defined if the rotation matrix is not given. Furthermore, as it is stated in section II.A, the θ_4 angle also forms a singularity issue concerning the 3D positioning of end effector, because it only affects the orientation of the Robolinks' endpoint. An end effector may require a specific range of θ_4 values to perform fruit picking, but the present study remains focused on the final position of the robotic arm.

III. Feedback Data Manipulation

A. Lidar Approach

The problem of recognizing an obstacle in order to avoid it, is similar to that of recognizing a target object (fruit) and then to pick it. Therefore, the Lidar-based setup and the indoor experiments had mainly the goal to investigate the behavior of Robolink during motion and its suitability to approach a given point avoiding the surrounding walls. Lidar is a Time of Flight (TOF) sensor that uses an edge emitting, 905nm, single stripe laser. The sensor includes a detector based on a Si PIN diode to receive the transmitted signal. Time delay is acquired by the argument of the maximum of the cross-correlation between a stored transmit reference (x_1) and the received signal (x_2) as it is described in (7),(8),

$$\tau_{delay}=\arg_t\max[(x_1*x_2)(t)] \quad (7)$$

and

$$(x_1*x_2)(\tau)=\int_{-\infty}^{\infty} x_1(t)x_2(t-\tau)dt \quad (8)$$

In the indoor experimental setup, the Lidar sensor is utilized to measure the distance from the walls that surround the workspace of Robolink in order to calculate the angles of its joints. Each Lidar is attached to a specific point so that the geometrical characteristics of Robolink make the calculation of the real value of each DoF convenient.

The first Lidar is located on the second link of the robot and it is parallel to that link structural axis. In the ABC triangle which is illustrated in Fig. 4, φ_1 angle is defined as,

$$\varphi_1=\arccos\frac{|AC|}{|AB|} \quad (9)$$

where |AB| is the measure result from the first Lidar increased by the factor of distance between Lidar and point A. |AC| is the distance from the center of pivoting to vertical and upper wall, respectively. It should be denoted that the origin of Robolink is prearranged to be located so that the distance from that point to the upper wall is equal to the one from the same point to the vertical wall. In other words, |AC| is common both in Fig. 4a and 4b.

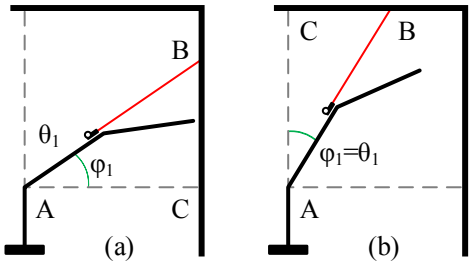

Figure 4. (a) Lidar faces vertical wall (b) Lidar faces upper wall.

When the first Lidar aims to the vertical wall (Fig. 4a),

$$\theta_1=90°-\varphi_1 \quad (10)$$

If it aims to the upper wall (Fig. 6b),

$$\theta_1=\varphi_1 \quad (11)$$

The second Lidar is placed vertically to the second link of the robotic manipulator in order to calculate the angle of the first rotational joint, then

$$\theta_2=\arccos\frac{x_{wall}}{L_2^{dist}} \quad (12)$$

where x_{wall} is the distance from the origin to the vertical wall which is a constant variable and L_2^{dist} is the measure result from the second Lidar.

The third Lidar is parallel to third link structural axis. In the DEF triangle (Fig. 5) the φ_3 angle is calculated,

$$\varphi_3=\arccos\frac{|DE|}{|DF|} \quad (13)$$

where |DE| and |DF| are defined in the same way as for the case of the first Lidar.

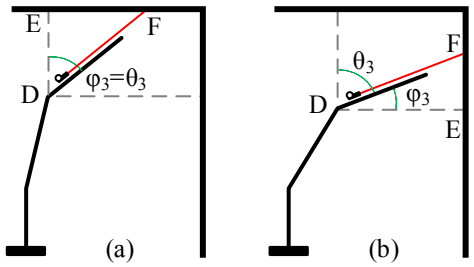

Figure 5. (a) Lidar faces upper wall (b) Lidar faces vertical wall.

When the third Lidar aims to the upper wall, θ_3 equals to φ_3 (Fig. 5a). Assuming that it aims to the vertical wall (Fig. 5b), θ_3 is calculated by (14),

$$\theta_3=90°-\varphi_3 \quad (14)$$

B. Kinect Sensor Approach

Microsoft Kinect is an RGB-Depth sensor, which utilizes a couple of IR receiver and emitter to measure depth distances in accordance to RGB pixels [29]. In this approach of acquiring the real values of θ_1, θ_2 and θ_3, Kinect sensor is not integrated on the robot arrangement but monitors the Robolink from an external place. Specifically, the sensor is placed in parallel to xz-plane of the origin coordinate system and is programmed to segment specific points of Robolink. Two templates of different colors are attached at the end of the second and third link respectively as shown in Fig. 6. Under these circumstances, the recognition of each DoF becomes convenient, regardless of the unmapped environment that surrounds Robolink.

It should be noted that Robolink has encoders in all joints for determination of their coordinates. Hence, the aim of using Kinect measurements was to test its recognition capabilities and mainly the accuracy and reliability of measurements in relation to the position tracking and control problem. Furthermore, it has been considered that the problem of end effector position tracking is similar to that of fruit tracking and picking, in the sense that tracking the position of the end effector using Kinect implies that the distance between the end effector and the fruit can be measured. In other words, when a fruit is identified in the Kinect scene, its coordinates could be calculated so as to trigger Robolink to pick it. Of course, the task of fruit recognition is a different and separate problem.

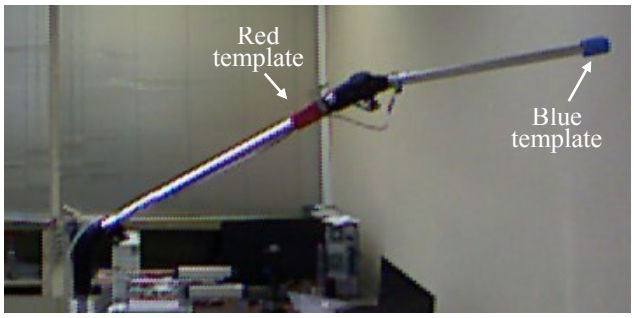

Figure 6. Red & Blue templates are attached on Robolink.

The position (x_p,y_p) of the red template on the RGB image can be extracted with the use of a color matching algorithm. Based on the triangle that it is created as illustrated in Fig. 7, θ_1 can be easily calculated as,

$$\theta_1=180-2\text{atan}\frac{|x_{red}-x^0_{red}|}{|y_{red}-y^0_{red}|} \quad (15)$$

where (x_{red}, y_{red}) is the location of the red template at random position and (x^0_{red}, y^0_{red}) is the position for $\theta_1=0$ which is constant.

To calculate θ_2 and θ_3 angles, coordinates of end effector in 3D space have to be already known. Position of the blue template in RGB frame (Fig. 6) can be recognized in the same way as the red one. This position corresponds to a specific pixel

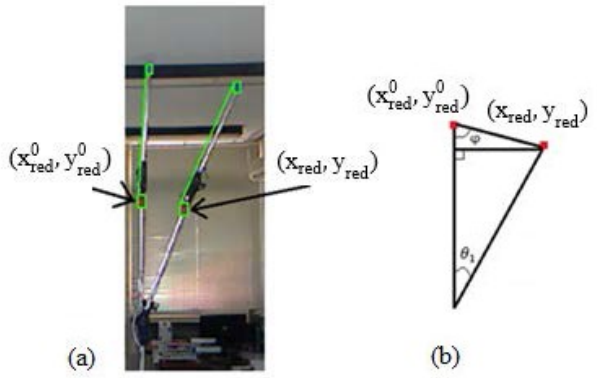

Figure 7. Triangle is defined by robot links among initial and random arrangement. Live Animation (a) – Geometrical Representation (b).

of the depth frame. Kinect measures the distance between itself and the scene objects for each pixel of the depth frame. In other words, depth measurements per frame are instantly saved into a matrix, which is called Depth Array. Real world coordinates can be given from (16) with reference to Kinect coordinate system,

$$\begin{bmatrix}x\\y\\z\end{bmatrix}=\begin{bmatrix}(\frac{r_x}{2}-x)\,d\,\frac{1}{f_x}\\(\frac{r_y}{2}-y)\,d\,\frac{1}{f_y}\\d\end{bmatrix} \quad (16)$$

where d is measurement of depth and (r_x,r_y) and (f_x,f_y) are resolution and focal length parameters of depth camera respectively.

It should be mentioned that RGB and depth frames are not perfectly aligned. To overcome that issue an algorithm, which performs the appropriate shift of the RGB pixel and validates the depth data has been developed.

Coordinates of the end effector can be easily transformed from Kinect coordinate system to the origin one. Given the angle θ_1 and x,y,z coordinates, (1) is simplified as,

$$\begin{bmatrix}x\\y\\z\end{bmatrix}=\begin{bmatrix}C_4+C_5\cos\theta_3+C_6\cos\theta_2\sin\theta_3\\C_2\sin\theta_2\sin\theta_3\\C_7+C_6\cos\theta_3-C_5\cos\theta_2\sin\theta_3+C_1\end{bmatrix} \quad (17)$$

where constants are defined as $C_4=C_1\sin\theta_1$, $C_5=C_2\sin\theta_1$, $C_6=C_2\cos\theta_1$ and $C_7=C_1\cos\theta_1$.

The linear combination of first and third equation of (17) becomes:

$$\begin{cases}C_5(x-C_4)=C_5^2\cos\theta_3+C_5C_6\cos\theta_2\sin\theta_3\\C_6(z-C_7-0{,}775)=C_6^2\cos\theta_3-C_5C_6\cos\theta_2\sin\theta_3\end{cases}\overset{+}{\Rightarrow}$$

$$C_5(x-C_4)+C_6(z-C_7-C_3)=(C_5^2+C_6^2)\cos\theta_3 \quad (18)$$

Equation (18) is simplified and θ_3 is calculated as:

$$\theta_3=\arccos\frac{C_5(x-C_4)+C_6(z-C_7-C_3)}{C_2^2} \quad (19)$$

Concerning θ_2, it is computed by substituting (19) to (17)

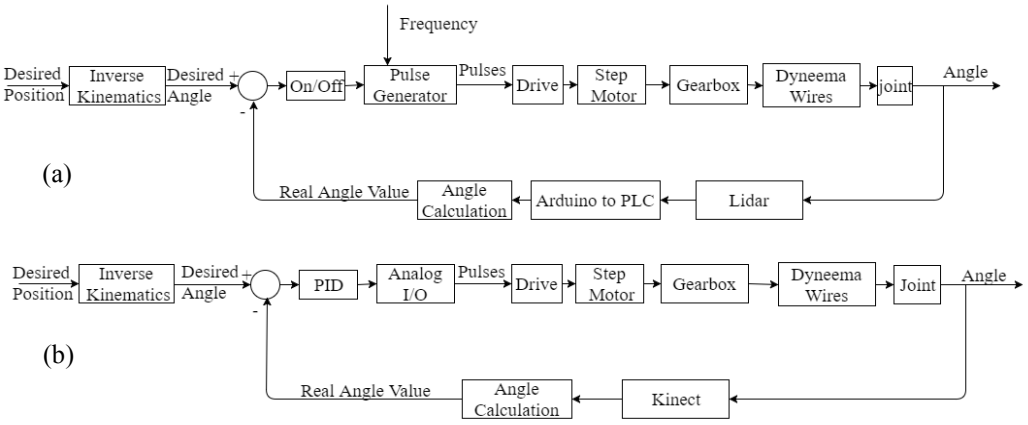

Figure 8. (a) Closed loop diagram for Lidar–PLC setup, (b) closed loop diagram for Kinect-LabVIEW setup.

$$\begin{cases} \cos\theta_2 = \dfrac{x - C_4 - C_5\cos\theta_3}{C_6\sin\theta_3} \\ \sin\theta_2 = \dfrac{y}{C_2\sin\theta_3} \end{cases} \quad (20)$$

$$\theta_2 = \text{atan2}(\sin\theta_2, \cos\theta_2) \quad (21)$$

IV. Setup Of Automatic Control

The configuration of automation task in aforementioned two stages of experimentation is discussed in this section. Basic components of control methods are depicted in schematic diagrams of Fig. 8. In the first setup (Fig. 8a), the automation process is executed by a PLC. The desired position of Robolink is given in [x,y,z] coordinates and then the desired angles [θ_1 θ_2 θ_3] are calculated through inverse kinematics. The data from the Lidar sensors are acquired by an Arduino Mega board and sent to the PLC so as to calculate the real angles, as it is explained in the previous section. Error signal is derived from the comparison between desired and real angle. The PLC produces a direction signal for each motor that defines the motor's direction and a movement signal that permits or denies externally generated pulses to be fed to the step motor. A pulse generator produces the pulses with a prefixed frequency and as a result, the shaft speed of each motor cannot be changed. Consequently, the ON-OFF control have been implemented. Each motor rotates until the deviation between the desired and real angle is inside a defined dead band (± 3˚ from the desired angle).

In the second setup (Fig. 8b), the automation process is designed and being monitored through the LabVIEW environment on a regular PC. User enters the desired position of Robolink giving either [x,y,z] coordinates or [θ_1,θ_2,θ_3] angles directly. In a real fruit picking system, these data will be given by the fruit recognition unit. Error signal occurs after the comparison between desired and real angle that is acquired from feedback loop as it is explained in the previous section. A PID controller leads an analog I/O board to feed pulses to the correspondent step motor. Relations between output angular movement and parameters of the experimental equipment such as tensionable drive wheel, gearhead, and Dyneema wires transposition are integrated into this model. As a result, a more accurate composition of control signals can be achieved. Shaft speed of each motor is regulated by the frequency of pulses. In this work, an algorithm decides the appropriate frequency in relation to the number of steps which have to be done. Thereby, this type of escalation combines high-speed movements and a smooth approach of equilibrium point.

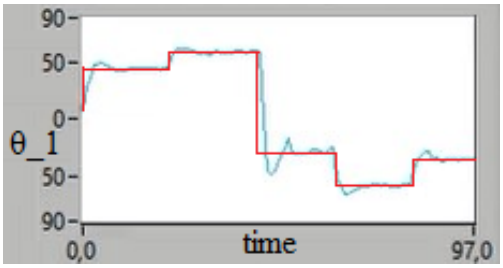

Figure 9. Response of θ_1 (blue line) – desired angle (red line).

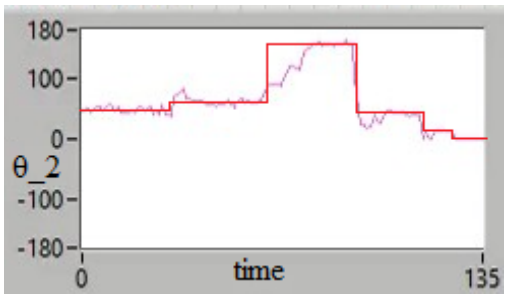

Figure 10. Response of θ_2 (purple line) – desired angle (red line).

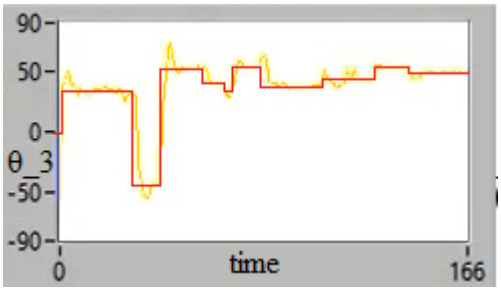

Figure 11. Response of θ_3 (yellow line) – desired angle (red line).

The PID controllers regulate each DoF response. As it is depicted in Figures 9-11, the system is sufficiently stabilized, according to the desired input. The I-component could be eliminated to zero. A new PD controller could be proven satisfying because overshooting would be minimized, although the residual state error would be negatively affected.

IV. CONCLUSION

The main contribution of this paper is the use of the Kinect sensor incorporated in a basic feedback position control law of a robotic articulated arm for tracking and control of its movement. The sensor monitors the robotic manipulator from an external point of view, just as it will do in recognizing a fruit and driving the arm to pick it. Lidar sensors, attached on the links of the robotic arm, have been also used for indoor experimentation on the manipulator kinematic behavior in respect to preset surrounding walls.

The basic joint's angles are calculated without requiring any specific initial positioning of the robotic arm and the Kinect based measurements are accurate in comparison to the encoders' ones. Therefore, from the position tracking and control side of view, the aforementioned Kinect-based technique applied on the specific Robolink arm is promising for using in fruit picking task. However, it should be tested on real fruit picking, where the work of direct recognition of the fruit will be added.

REFERENCES

[1] M. W. Spong, "Modeling and control of elastic joint robots," Journal of Dynamic Systems, Measurement, and Control, vol. 109, no. 4, p. 310, 1987

[2] F. Ghorbel, J. Y. Hung, and M. W. Spong, "Adaptive control of flexible-joint manipulators," IEEE Control Systems Magazine, vol. 9, no. 7, pp. 9–13, Dec. 1989.

[3] K. Khorasani, "Adaptive control of flexible-joint robots," IEEE Transactions on Robotics and Automation, vol. 8, no. 2, pp. 250–267, Apr. 1992.

[4] S. S. Ge, "Adaptive controller design for flexible joint manipulators," Automatica, vol. 32, no. 2, pp. 273–278, Feb. 1996.

[5] V. Zeman, R. V. Patel, and K. Khorasani, "A neural network based control strategy for flexible-joint manipulators," Proceedings of the 28th IEEE Conference on Decision and Control, pp. 1759–1764, Dec. 1989.

[6] S. S. Ge and I. Postlethwaite, "Adaptive neural network controller design for flexible joint robots using singular perturbation technique," Transactions of the Institute of Measurement and Control, vol. 17, no. 3, pp. 120–131, Aug. 1995.

[7] F. Abdollahi, H. A. Talebi, and R. V. Patel, "A stable neural network-based observer with application to flexible-joint manipulators," IEEE Transactions on Neural Networks, vol. 17, no. 1, pp. 118–129, Jan. 2006.

[8] S. J. Yoo, J. B. Park, and Y. H. Choi, "Adaptive dynamic surface control of flexible-joint robots using self-recurrent Wavelet neural networks," IEEE Transactions on Systems, Man and Cybernetics, Part B (Cybernetics), vol. 36, no. 6, pp. 1342–1355, Dec. 2006

[9] W. Khalil and S. Besnard, "Geometric Calibration of Robots with Flexible Joints and Links," Journal of Intelligent and Robotic Systems, vol. 34, no. 4, pp. 357–379, 2002.

[10] A. K. Kostarigka, Z. Doulgeri, and G. A. Rovithakis, "Prescribed performance tracking for flexible joint robots with unknown dynamics and variable elasticity," Automatica, vol. 49, no. 5, pp. 1137–1147, May 2013.

[11] F. T. Mrad and S. Ahmad, "Adaptive control of flexible joint robots using position and velocity feedback," International Journal of Control, vol. 55, no. 5, pp. 1255–1277, May 1992

[12] M. Jankovic, "Observer based control for elastic joint robots," IEEE Transactions on Robotics and Automation, vol. 11, no. 4, pp. 618–623, 1995.

[13] M. Oya and M. Wada, "Simple robust tracking controller for rigid link flexible joint robots using only joint position and velocity measurements," SICE 2000. Proceedings of the 39th SICE Annual Conference, Iizuka, Japan, pp. 79–84, 2000

[14] Hirzinger, A. Albu-Schaffer, M. Hahnle, I. Schaefer, and N. Sporer, "On a new generation of torque controlled light-weight robots," Proceedings 2001 ICRA. IEEE International Conference on Robotics and Automation, May 2001.

[15] L. Le Tien, A. Albu-Schaffer, A. De Luca, and G. Hirzinger, "Friction observer and compensation for control of robots with joint torque measurement," 2008 IEEE/RSJ International Conference on Intelligent Robots and Systems, Sep. 2008.

[16] J. Klodmann, R. Konietschke, A. Albu-Schaffer, and G. Hirzinger, "Static calibration of the DLR medical robot MIRO, a flexible lightweight robot with integrated torque sensors," 2011 IEEE/RSJ International Conference on Intelligent Robots and Systems, Sep. 2011.

[17] S. Nicosia and P. Tomei, "A tracking controller for flexible joint robots using only link position feedback," IEEE Transactions on Automatic Control, vol. 40, no. 5, pp. 885–890, May 1995.

[18] S. Y. Lim, D. M. Dawson, J. Hu, and M. S. de Queiroz, "An adaptive link position tracking controller for rigid-link flexible-joint robots without velocity measurements," IEEE Transactions on Systems, Man and Cybernetics, Part B (Cybernetics), vol. 27, no. 3, pp. 412–427, Jun. 1997.

[19] Y. Chang and H. Yen, "Design of a robust position feedback tracking controller for flexible-joint robots", IET Control Theory & Applications, vol. 5, no. 2, pp. 351–363, Jan. 2011.

[20] G. Muscato, M. Prestifilippo, N. Abbate, and I..Rizzuto, "A prototype of an orange picking robot: past history, the new robot and experimental results", Industrial Robot: An International Journal, Vol. 32 Issue: 2, pp.128-138, 2005.

[21] A. J. Scarfe, R. C. Flemmer, H. H. Bakker, and C. L. Flemmer, "Development of an autonomous kiwifruit picking robot", 4th International Conference on Autonomous Robots and Agents, ICARA'09, 10-12 Feb. 2009.

[22] J. Baeten, K. Donne, S. Boedrij, W. Beckers, and E. Claesen. "Autonomous Fruit Picking Machine: A Robotic Apple Harvester", 6th International Conference on Field and Service Robotics, FSR'07, pp.1-9, Jul. 2007.

[23] T. R. Vittor, R. Willgoss, and T. Furukawa, "Modular Decentralized Control of Fruit Picking Redundant Manipulator", Australian Conference on Robotics and Automation, Brisbane, pp. 1-8, Dec. 2003.

[24] A. J. Kurhade, A. M. Deshpande, and R. D. Dongare, "Review on Automation in Fruit Harvesting", International Journal of Latest Trends in Engineering and Technology, Vol. 6, Issue 2, pp.1-15, Nov. 2015.

[25] D. Font, T. Pallejà, M. Tresanchez, D. Runcan, J. Moreno, D. Martínez, M. Teixidó, and J. Palacín, "A Proposal for Automatic Fruit Harvesting by Combining a Low Cost Stereovision Camera and a Robotic Arm", Sensors International Journal, Vol. 14, Issue 7, pp. 11557-579, Jun. 2014.

[26] S. Konam, "Agricultural Aid for Mango cutting" (AAM), International Conference on Advances in Computing, Communications and Informatics, ICACCI'14, pp.1520-24, Sept. 2014.

[27] C. S. Nandi, B. Tudu, and C. Koley, "Machine vision based automatic fruit grading system using fuzzy algorithm", International Conference on Control, Instrumentation, Energy and Communication, CIEC'14, pp.76-80, Feb. 2014.

[28] M. W. Spong, M. Vidyasagar, and M. Vidyasagar, Robot dynamics and control. New York: John Wiley and Sons (WIE), 1989.

[29] B. Karan, "Calibration of Kinect-type RGB-D sensors for robotic applications," FME Transaction, vol. 43, no. 1, pp. 47–54, 2015.